Microchim Acta (2017) 184:3291–3299
DOI 10.1007/s00604-017-2344-7

ORIGINAL PAPER

Amperometric detection of nitric oxide using a glassy carbon electrode modified with gold nanoparticles incorporated into a nanohybrid composed of reduced graphene oxide and Nafion

Norazriena Yusoff[1] · Perumal Rameshkumar[1,2] · Muhammad Mehmood Shahid[1] · Sheng-Tung Huang[3] · Nay Ming Huang[4]

Received: 8 March 2017 / Accepted: 26 May 2017 / Published online: 6 June 2017

Abstract The authors show that the electrocatalytic performance toward the detection of nitric oxide (NO) can be enhanced by making use of gold nanoparticles (AuNP) in a matrix consisting of reduced graphene oxide and Nafion (rGO-Nf). The rGO-Nf@Au nanohybrid was synthesized via a hydrothermal method. The spherical AuNP have diameters in the range from 50 to 200 nm as proven by field emission scanning electron microscopy (FESEM). A glassy carbon electrode (GCE) modified with the nanohybrid displays excellent electrocatalytic activity towards NO oxidation compared to other kinds of modified electrodes. Best operated at a voltage of +0.8 V (vs. SCE), the amperometric response was linear in the 1 μM to 0.16 mM nitrite concentration range, with 0.5 μM detection limit (at an S/N ratio of 3). The high surface area of the AuNP along with the synergistic effect of AuNP and rGO-Nf film on the signal current is believed to cause the enhanced electrocatalytic activity of the nanohybrid. The sensor is not interfered by dopamine (DA), ascorbic acid (AA), uric acid (UA), glucose, urea, and NaCl even in 5-fold higher concentrations. In our perception, the rGO-Nf@Au modified electrode is a promising tool for highly sensitive and selective amperometric sensing of NO.

Keywords Graphene materials · Metal nanoparticles · Electrochemical sensor · Modified electrode · Electroanalysis · Biomolecules

Electronic supplementary material The online version of this article (doi:10.1007/s00604-017-2344-7) contains supplementary material, which is available to authorized users.

✉ Perumal Rameshkumar
rameshkumar.p@klu.ac.in

✉ Nay Ming Huang
huangnayming@gmail.com

[1] Low Dimensional Materials Research Centre, Department of Physics, Faculty of Science, University of Malaya, 50603 Kuala Lumpur, Malaysia

[2] Department of Chemistry, Kalasalingam University (Kalasalingam Academy of Research and Education), Krishnankoil, Tamil Nadu 626 126, India

[3] Institute of Biochemical and Biomedical Engineering, National Taipei University of Technology, Taipei, Taiwan, Republic of China

[4] Faculty of Engineering, Xiamen University of Malaysia, Jalan Sunsuria, Bandar Sunsuria, 43900 Sepang, Selangor Darul Ehsan, Malaysia

Introduction

Nitric oxide (NO) is one of the labile free radicals and hydrophobic molecules that are being produced by the human body. In 1987, a research led by Ignarro had discovered that NO is responsible for the vascular smooth muscle relaxation elicited by endothelium-derived relaxing factor [1]. Later research successfully proved the involvement of NO in a range of defence stress responses and its ability to alleviate the deleterious effects of regulating reactive oxygen species (ROS) by regulating ROS production and degradation [2]. Moreover, NO is also used for communication between cells and is involved in the regulation of blood pressure, the immune response, platelet aggregation and clotting, and neurotransmission [3]. The concentration of NO in exhaled breath is also used as a biomarker for several diseases such as asthma [4], ulcerative colitis and Crohn's disease [5]. The determination of NO is significant because the abnormality of its production and bioavailability may led to several diseases such as obesity, diabetes (both type I and II), atherosclerosis,

hypertension, and heart failure [6, 7]. Therefore, the fabrication of a sensor which has a compact design and highly sensitive and selective toward NO is important as it can make a great contribution to disease diagnosis.

One of the effective ways to determine NO is by using electrochemical technique [8]. Electrochemical detection has been a primary method for monitoring neurotransmitters in vivo due to its simplicity, long term high stability, fast response, low cost, and higher level of sensitivity and selectivity. NO is an electro active molecule and can be detected electrochemically. Graphene incorporated with metal/metal oxide nanoparticles has attracted much attention for modifying the electrode surface because these nanocomposites exhibit unique properties which cannot be found in conventional materials [9, 10]. Hu et al. successfully synthesized reduced graphene oxide-ceria (rGO–CeO_2) nanocomposite nanostructures which offered a facile and reliable platform to in situ real-time detect bio-signal NO molecules released by living cells [11]. The improvement in the sensing performance was believed to the synergical effect from high catalytic activity of the specifically shaped CeO_2 nanocrystal and good conductivity and high surface area of rGO. Our research group had used reduced graphene oxide-cobalt oxide nanocube@platinum (rGO–Co_3O_4@Pt) nanocomposite as the active material for the detection of in situ generated NO [12]. The high catalytic effect of the rGO–Co_3O_4@Pt nanocomposite was attributed to the synergistic effect of Co_3O_4 nanocubes and Pt nanoparticles present in the rGO matrix, which then contributed to a better sensing performance.

In this study, one step hydrothermal method was employed to obtain rGO-Nf film doped with AuNP. The rGO-Nf@Au nanohybrid has been used as the active material for modifying the GCE. This modified electrode was used in detecting NO using electrochemical method. Three different concentrations of $HAuCl_4.3H_2O$ were used in order to study the effect of AuNP content on the electrochemical sensing performance.

Experimental

Materials

Graphite flakes was purchased from Asbury Graphite Mills, Inc. (www.asbury.com). Sulphuric acid (H_2SO_4, 95 ~ 97%), phosphoric acid (H_3PO_4), hydrochloric acid (HCl, 37%), urea, 3-hydroxytyraminium chloride, and ammonia solution (NH_4OH) were received from Merck (www.merck.com). Potassium permanganate ($KMnO_4$) was obtained from R&M chemicals (www.evergainful.com.my). Nafion (200 mesh) was purchased from Ion Power, Inc. (www.nafionstore.com). Gold(III) chloride trihydrate ($HAuCl_4.3H_2O$) was purchased from abcr.Gmbh & Co. KG (www.abcr.de). Hydrogen peroxide (H_2O_2) and ethanol were received from Systerm (www.haiousaintifik.com). Sodium phosphate monobasic (NaH_2PO_4), disodium phosphate dihydrate ($Na_2HPO_4.2H_2O$), sodium nitrite ($NaNO_2$), uric acid (UA), glucose, sodium chloride (NaCl), and L(+)-ascorbic acid were obtained from Sigma-Aldrich (www.sigmaaldrich.com). Aqueous solutions were prepared in double distilled water. All chemicals and solvents were used without any further purification unless otherwise stated.

Characterization techniques

The crystalline phases of the samples were collected with X-ray diffraction (XRD; PANalytical Empyrean), using copper Kα radiation (λ = 1.5418 Å) at a scan rate of 0.02 s^{-1} (www.dksh.com). Raman spectrum of the nanohybrid was collected using a Renishaw inVia Raman microscope linked to the 514 nm line of an argon ion laser as the excitation source and performed at room temperature (www.renishaw.com). X-ray photoelectron spectroscopy (XPS) was measured at the beam-line, BL3.2 (a) of the Synchrotron Light Research Institute in Thailand using a Thermo VG Scientific-Alpha110 electron energy analyzer (www.thermofisher.com). It was operated under the condition of photon energy of 600 eV with 0.1 eV kinetic energy steps. The morphologies and the energy-dispersive X-ray (EDX) analyses of the samples were examined using a Hitachi SU8030 field emission scanning electron microscope (FESEM) which equipped with EDX, operated at 5.0 kV (www.hitachi-hightech.com). The nanohybrid materials were drop-casted on a silicon wafer, which was used as the substrates for FESEM characterization.

Synthesis of rGO-Nf@Au nanohybrid

The rGO-Nf@Au nanohybrid was prepared using hydrothermal method. In the first step, GO-Nf solution was prepared using ultrasonication method according to the procedure reported previously [13]. Next, the aqueous mixture was prepared by mixing 20 mL of GO-Nf solution and 2 mL of $HAuCl_4.3H_2O$ solution. Above mixture was then stirred for 15 min at room temperature. For a control experiment, three different concentrations of $HAuCl_4.3H_2O$ (4, 8, and 12 mM) were used. Then, 13 mL of NH_4OH were slowly added into the solution while stirring to avoid sudden agglomeration. Prior to transferring to a Teflon-lined autoclave, the solution mixture was homogeneously stirred for 20 min. The hydrothermal synthesis was carried out at temperature of 180 °C for 16 h and subsequently cooled down to room temperature naturally after the reaction. Afterwards, the black precipitate was collected by centrifugation and washed with distilled water and ethanol for several times, and dried at 60 °C in the oven for 24 h. Ammonia acted as the reducing agent for the formation of AuNP and rGO at a given temperature. The powder was labelled as rGO-Nf@Au4, rGO-Nf@Au8, and rGO-

Nf@Au12 nanohybrids which referred to the usage of 4, 8 and 12 mM of $HAuCl_4.3H_2O$, respectively.

Fabrication of GC/rGO-Nf@Au modified electrode

The GCE was polished with 0.05 μm alumina slurry on a polishing cloth for a few times before rinsed with distilled water. Then, the electrode was undergone pretreatment by running 20 cycles of cyclic voltammetry (CV) at potential between +1 and −1 V in 0.1 M H_2SO_4 solution. A 5 mg of rGO-Nf@Au nanohybrid powder was dispersed in 5 mL of water with the aid of ultrasonic agitation to create a homogeneous suspension. After the cleaning process, a 5 μL of suspension was dropped onto the surface of GCE (dia. 3 mm) and the electrode was dried in air to form GC/rGO-Nf@Au modified electrode.

Electrochemical measurements

The electrochemical experiments were performed with a VersaSTAT 3 by Princeton Applied Research using a conventional three-electrode system (www.princetonappliedresearch.com). The GC/rGO-Nf@Au modified electrode was used as the working electrode, a saturated calomel electrode (SCE) as the reference electrode and platinum wire as the counter electrode. 0.1 M phosphate buffer with pH 2.5 was used as the supporting electrolyte and $NaNO_2$ was used as the precursor to generate the NO in the acidic solution. All electrochemical experiments were performed at room temperature. The schematic illustration for synthesizing rGO-Nf@Au nanohybrid and the fabrication of GC/rGO-Nf@Au modified electrode are shown in Scheme S1. For electrochemical impedance spectroscopy (EIS) measurement, the experiment was carried out in a solution containing 5 mM $K_3[Fe(CN)_6]^{3-/4-}$ and 0.1 M KCl within the frequency range from 0.01 Hz to 100 KHz.

Real sample analysis

The water samples used in this study were tap and lake water, which were collected from Low Dimensional Materials Research Centre's laboratory and University of Malaya's lake. Standard addition method was used to perform the recovery experiment. Before determination, the water samples were filtered to remove the suspended solid substances. A stock solution of NO_2^- was prepared by adding a known amount of $NaNO_2$ in 5 mL of real water samples and sonicated for 15 min. A known amount of those samples were spiked into 0.1 M PBS (pH 2.5) and the concentration of NO was determined from the current response obtained by amperometry experiment at an applied potential of +0.8 V (vs. SCE).

Results and discussion

Choice of materials

Inspired by the large surface area and unique conductivity of reduced rGO and the excellent electrocatalytic activity of AuNP, a nanohybrid consisting of rGO-Nf and AuNP was synthesized for the study of highly sensitive and selective electrochemical NO sensor. The use of Nafion as an ion exchange membrane enhances the surface area scaffold for the deposition and stabilization of AuNP and provides the ion conductive pathway during the electrochemical reaction.

Characterization of rGO-Nf@Au nanohybrid

The crystalline nature of rGO-Nf@Au nanohybrids with different Au content was analyzed using XRD and the results were shown in Fig. 1. In general, the XRD pattern for GO shows a characteristic diffraction peak at around 11 ° with an interlayer *d*-spacing of 8.36 Å (Fig. 1a) [14]. Upon the

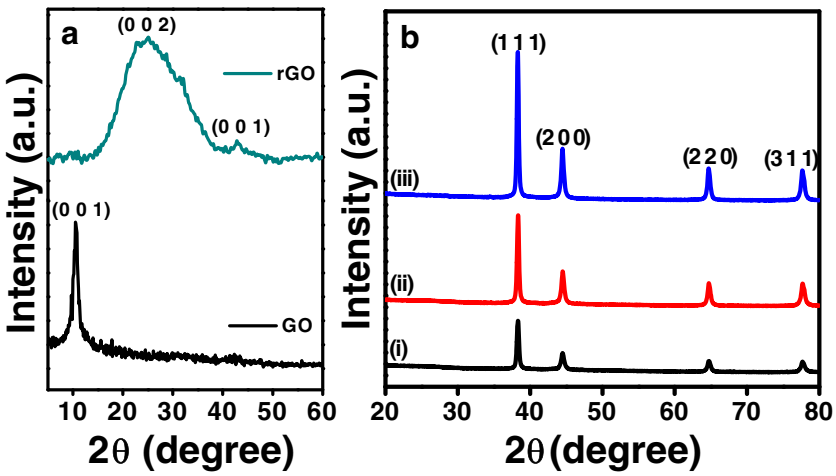

Fig. 1 XRD patterns of **(a)** GO and rGO. **b** XRD patterns of **(i)** rGO-Nf@Au4, **(ii)** rGO-Nf@Au8 and **(iii)** rGO-Nf@Au12 nanohybrids

hydrothermal treatment, this peak disappeared and a new broad peak emerges at round 25 ° which corresponds to the (0 0 2) plane of hexagonal graphene structure and thus, confirmed the formation of rGO. The band at 43 ° which appeared in XRD pattern for rGO corresponded to the turbostratic band of disordered carbon materials [15]. The decrease in *d*-spacing after hydrothermal reaction was due to the removal of the oxide functional groups in GO and to the restoration of the crystal structure of graphite after the reduction of GO via hydrothermal treatment. The XRD patterns for three different rGO-Nf@Au nanohybrids were displayed in Fig. 1b. The diffraction peaks observed at 38.29 °, 44.48 °, 64.68 °, and 77.68 ° were assigned to the (1 1 1), (2 0 0), (2 2 0), and (3 1 1) planes of Au, respectively [16]. All the peaks were well matched and consistent with the standard database (JCPDS card: 65–2870), and thus confirmed the existence of AuNP on the surface of rGO-Nf sheets. As can be seen, no rGO peak was observed in all XRD patterns of nanohybrids. This observation may have been due to the relatively lower diffraction intensity of rGO compared to AuNP. It suggested that the surface of the rGO-Nf was fully covered with AuNP. All the peaks are sharp, with high intensities and without impurity peaks. This proves the higher crystallinity and purity of the nanohybrid. The only notable difference between the XRD patterns of all three rGO-Nf@Au nanohybrids was the intensity of their peaks that increased with the increase in AuNP content from 4 to 12 mM. This result indicated that the existence of AuNP became dominant in the nanohybrid. This is because more AuNP were formed on the surface of rGO-Nf sheets when higher concentration of AuNP precursor was used.

A Raman scattering study was performed to confirm the presence of rGO in the nanohybrids. The detailed information was provided in the Supporting Information (Fig. S1). The presence of functional groups on the surfaces of rGO-Nf@Au nanohybrids were evaluated by XPS and the results are shown in Fig. 2. Fig. 2a shows the XPS peak deconvolution of C1s core levels of the rGO-Nf@Au nanohybrids. It was noted that two characteristic peaks of C-C and C-F were observed at binding energy of 284.5 and 291.1 eV, respectively. They attributed to the presence of rGO and Nafion in the nanohybrid material. One can also notice that the intensity of C-C peak for rGO-Nf@Au8 nanohybrid was the highest compared to other nanohybrids. The results demonstrated that the rGO in this nanohybrid has higher degree of reduction due to effective removal of oxygen functional groups after hydrothermal process. Fig. 2b presents the XPS spectrum of Au 4f core level in the rGO-Nf@Au nanohybrids. The deconvoluted peaks located at the binding energies of 83.8 and 87.5 eV were assigned to the Au $4f_{7/2}$ and Au $4f_{5/2}$, respectively [17]. Therefore, the XPS results further confirmed the formation of AuNP on the rGO-Nf surface.

The morphology of the rGO-Nf@Au nanohybrids was characterized using FESEM analysis. The detailed discussion on the results is provided in the Supporting Information (Fig. S2). The energy dispersive X-ray (EDX) elemental mapping analysis was employed to reveal the distribution of various elements present in the rGO-Nf@Au8 nanohybrid (Fig. 3**)**. The elemental mappings of C (green), O (blue), F (black), and Au (red) were observed, which reveal that these elements were uniformly distributed in the rGO-Nf@Au8 nanohybrid. The large area covered by red color indicated the successful deposition and distribution of Au in the rGO-Nf film. The strong signals of C, O, F, and Au elements in EDX spectrum further confirm the formation rGO-Nf@Au8 nanohybrid (Fig. S3).

Electrochemical oxidation of NO

A detailed discussion on the electrochemical impedance spectroscopy (EIS) analysis and CV characteristics of rGO-Nf@Au nanohybrid modified GCE are provided in the Supporting Information (Fig. S4). The electrocatalytic NO

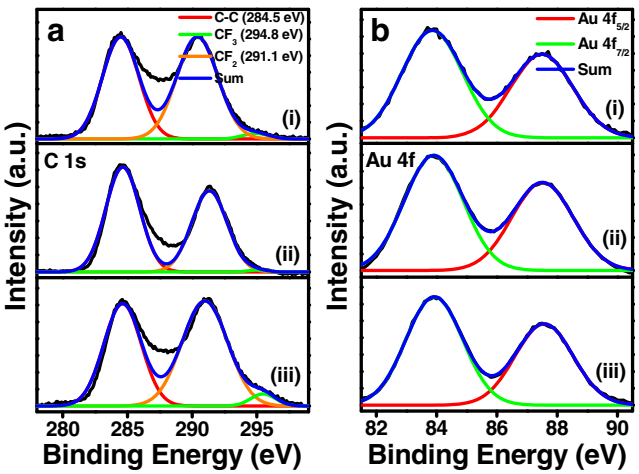

Fig. 2 XPS spectra of the **(a)** C1s and **(b)** Au 4f core level region for **(i)** rGO-Nf@Au4, **(ii)** rGO-Nf@Au8, and **(iii)** rGO-Nf@Au12 nanohybrids

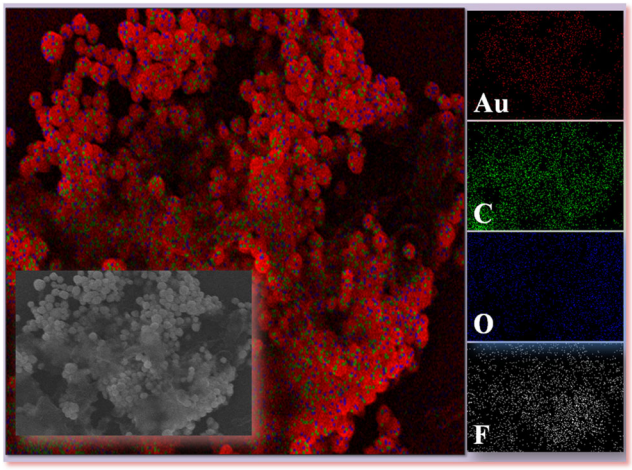

Fig. 3 EDX elemental mapping analysis. Inset shows the FESEM image of rGO-Nf@Au8 nanohybrid

oxidation at the rGO-Nf@Au nanohybrid modified electrode was investigated by recording the CV response. In order to produce NO in acidic solution, sodium nitrite ($NaNO_2$) was used as the precursor where it undergoes disproportionation reaction in acidic solution (pH ≤4) to generate free NO (Eq. (1) and (2)) [18]. The concentration of NO was determined by controlling the concentration of the $NaNO_2$ injected into the bulk electrolyte solution at pH 2.5.

$$2NaNO_2 + H_2SO_4 \rightarrow 2HONO + Na_2SO_4 \quad (1)$$

$$3HONO \rightarrow H^+NO_3^- + 2NO + H_2O \quad (2)$$

Figure 4 compares the CV curves of all the modified electrodes investigated in this work towards the oxidation of 1 mM NO_2^- in 0.1 M phosphate buffer (pH 2.5) with the rate of 50 $mV.s^{-1}$. Upon the addition of 1 mM NO_2^- in the solution, an anodic peak current occurred in CV curves for bare GC and other modified electrodes. Each electrodes shows different amount of current response and peak position (Fig. 4a). This anodic peak was assigned to the oxidation of NO at the surface of sensor electrode. As can be seen in Fig. 4b, the GC/rGO-Nf@Au8 modified electrode shows higher anodic peak current for the oxidation of NO compared to bare GC and other modified electrodes. This observation suggested that the incorporation of 8 mM AuNP with rGO-Nf

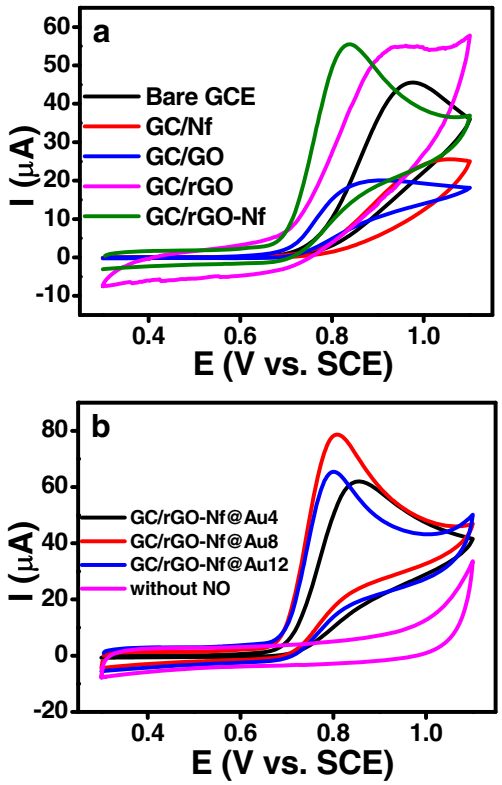

Fig. 4 **a** and **b** CV curves recorded at different modified electrodes for 1 mM of NO_2^- in 0.1 M phosphate buffer (pH 2.5) at a scan rate of 50 $mV.s^{-1}$

has significantly improved the performance of the electrode toward NO oxidation. The current response for each sensor electrode increased follows the order of: GC/GO < GC/Nf < Bare GC < GC/rGO < GC/rGO-Nf < GC/rGO-Nf@Au4 < GC/rGO-Nf@Au12 < GC/rGO-Nf@Au8. The low current response shown by GC/GO and GC/Nf compared to bare GC can be explained by the weak electrical conductivity of GO and Nf which affecting the rate of electron transfer. The high current response was due to the enhancement in the electron transfer kinetics at the GC/rGO-Nf@Au8. It was driven by the excellent electrical conductivity of rGO and AuNP as well as large amount of active surface area on the modified electrode. There was no apparent oxidation peak in the CV curve of rGO-Nf@Au8 was observed in the absence of NO in the solution as shown in Fig. 4b. The effects of changing concentration of NO_2^- and scan rate on the electrooxidation of NO at the nanohybrid modified electrode are discussed in Supporting Information (Fig. S5 & S6).

Amperometric detection of NO

The information on repeatability, reproducibility, and stability of the sensor electrode is provided in Supporting Information (Fig. S7). The electrochemical NO sensors were fabricated and tested accordingly in order to examine the application of the rGO-Nf@Au nanohybrids. For an explicit comparison, the amperometric responses were recorded at different modified electrode in 0.1 M phosphate buffer (pH 2.5) with successive addition of 50 μM NO_2^- and plotted in Fig. 5. After the addition of 50 μM NO_2^-, an increase in the current response with increasing NO_2^- concentration was detected for all modified electrode as can be seen in Fig. 5a. This result reveals that the GC/rGO-Nf@Au8 modified electrode provides more amplified responses than bare GC and other modified electrodes. The calibration plots from the amperometric responses were presented in Fig. 5b. The enhancement of analyte interaction surface area and high electrical conductivity provided by rGO-Nf@Au8 nanohybrid contribute to the improvement in sensing performances of the GC/rGO-Nf@Au modified electrode over the other modified electrodes. However, the overloaded AuNP content in the nanohybrid (rGO-Nf@Au12), the AuNP may form agglomeration and increase the diffusion layer thickness, therefore reducing the electron transfer rate, thus lower the sensitivity of the sensor electrode. To put these results in perspective, the sensitivity of GC/rGO-Nf@Au8 modified electrode is the larger than other modified electrode. Therefore, this sensor electrode was chosen for further study in determine the low detection limit for NO in acidic solution.

The amperometry was performed at an applied potential of +0.8 V (vs. SCE) for different NO_2^- concentrations in order to investigate the concentration detection limits for GC/rGO-Nf@Au8 modified electrode and was plotted in Fig. 5c. Figure 5c shows an excellent amperometric response with

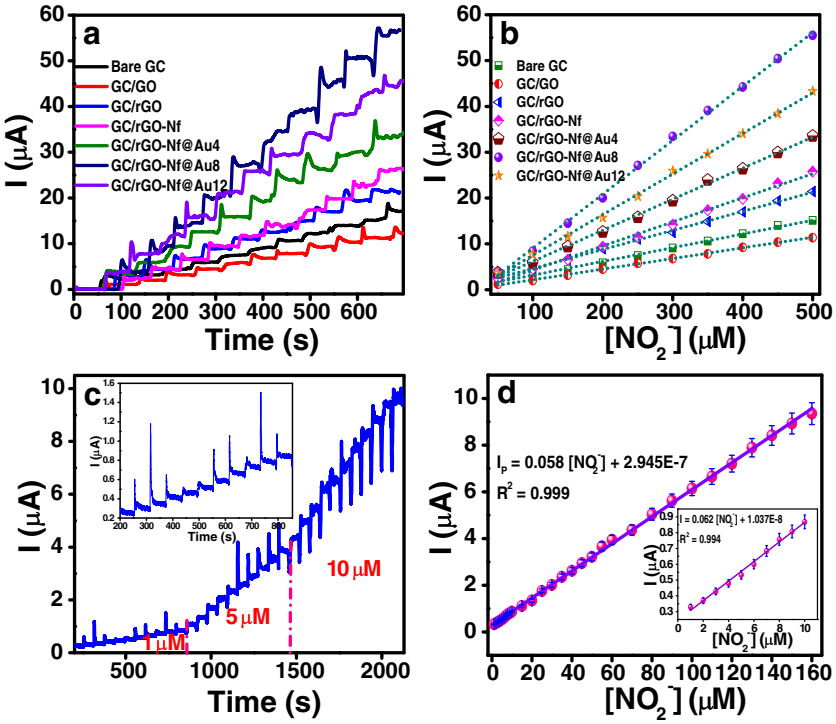

Fig. 5 **a** Amperometric I-t curves of different modified electrodes to subsequent additions of 50 μM NO_2^- in 0.1 M phosphate buffer (pH 2.5) at an applied potential of +0.8 V (vs. SCE). **b** The corresponding calibration curve of current versus concentration of NO_2^- for different modified electrode. **c** Amperometric (I-t) response of GC/rGO-Nf@Au8 modified electrode in 0.1 M phosphate buffer (pH 2.5) at an applied potential of +0.8 V (vs. SCE) upon successive additions of different concentration of NO_2^- in a step of 1, 5, and 10 μM. Inset shows the I-t response from 200 to 850 s. **d** The corresponding calibration curve of current versus concentration of NO_2^-. Inset shows the enlargement of the calibration curve from 1 to 10 μM of NO_2^- concentration

successive additions of different NO_2^- concentration for every 60 s recorded at GC/rGO-Nf@Au8 modified electrode. Upon the injection of NO_2^- in the solution, a significant increase in the current response with increase in the concentration of NO_2^- was observed. The current response against the NO_2^- concentration in the response time ranging from 200 to 850 s was shown in **inset of** Fig. 5c. Interestingly, the response time of the modified electrode was recorded to be within a second. It indicates the rapid diffusion of NO on the GC/rGO-Nf@Au8 modified electrode surface; thereby this sensor electrode can be used for real time measurements. It can also be notices that the oxidation current increases linearly with the successive addition of NO_2^- into phosphate buffer (Fig. 5d). The calibration curve between the peak currents and different NO_2^- concentrations in the range from 1 to 10 μM were showed in the **inset of** Fig. 5d. The linear regression equation was expressed as $I = 0.062\ [NO_2^-] + 1.037E{-}8$ ($R^2 = 0.994$) with the limit of detection of 5.0×10^{-7} M (S/N = 3). Table 1 presents the performance of the GC/rGO-Nf@Au8 modified electrode in comparison with other amperometric sensors for the detection of NO. By comparison, the NO sensor presented in this work exhibits a comparable sensing performance with other sensor electrodes. It was believed that the good synergetic effect between rGO-Nf and AuNP in forming the nanohybrids leads to the improvement in conductivity. As a result, the electron transfer resistance will reduce; hence increase the efficiency of the electron transfer between electrode and electrolyte. Moreover, the enhancement of the active surface area provided by rGO-Nf@Au8 nanohybrids allowed more analyte molecules to be interacted. These factors give a positive effect in sensing performance of GC/rGO-Nf@Au8 modified electrode especially in increase its sensitivity toward detecting of NO. The low detection limit and high sensitivity with fast response time demonstrated by GC/rGO-Nf@Au8 modified electrode shows the potentiality of the GC/rGO-Nf@Au8 as the alternative material for fabricating a sensor electrode for determining NO in biological analysis.

Selectivity of the sensor electrode

Some possible coexisting components such as DA, AA, UA, glucose, NaCl, and urea were examined in order to evaluate the selectivity of the constructed GC/rGO-Nf@Au8 modified electrode. Figure 6 shows the amperometric responses of GC/rGO-Nf@Au8 modified electrode for the successive additions of 1 μM NO_2^- and 10 μM DA, AA, UA, glucose, NaCl, and urea in 0.1 M phosphate buffer (pH 2.5). It was recorded at a regular interval of 60 s and an applied potential value of +0.8 V (vs. SCE). It can be seen that the aforementioned interference species did not produced any amperometric responses signals despite higher concentrations had been used. However, the apparent current increase can be observed with the instantaneous addition of NO_2^- in the same solution. This observation attests that GC/rGO-Nf@Au8 modified electrode exhibits favorable selectivity characteristics toward the detection of NO. These results suggest that rGO-Nf@Au8 showed potential applications for the detection of NO in real sample analysis

Table 1 Comparison in the sensing performance of GC/rGO-Nf@Au8 modified electrode with other reported sensor electrodes for the determination of NO

Electrode	Analytical method	Limit of detection (μM)	Sensitivity	Interferences	Reference
GC/Cyt c –SDS-PAM	Amperometry	0.1	-	DA, AA, K^+, Na^+, NH_4^+, Mg^{2+}, Al^{3+}, Ca^{2+}, Cu^{2+}, SO_4^{2-}, CO_3^{2-}, NO_3^-, Cl^-	[19]
ITO/MPTS-FAuNPs	Amperometry	0.00031	-	DA, AA, UA, cysteine, Na^+, K^+, Mg^{2+}, Ni^{2+}	[18]
Au/trans-$[Ru(NH_3)_4(Ist)(SO_4)]^+$	SWV	0.0773	-	DA, serotonin, NO_2^-	[20]
GC/Hb–CPB-PAM	CV	9.3	-	-	[21]
GC/Pt-Fe(III)	DPV	0.018	-	H_2O_2, DA, AA, UA, glucose, epinephrine, norepinephrine, L-glutamic acid, cysteine, D-fructose, sucrose, citric acid	[22]
GC/rGO-CeO_2	Amperometry	0.0096	1676.06 mA cm^{-2} M^{-1}	Ca^{2+}, K^+, Na^+, CO_3^{2-}, NO_3^-, Cl^-, UA	[11]
PG/ Hb-sodium montmorillonite	CV	0.002	-	DA, ascorbate, UA, NO^{2-}, epinephrine	[23]
PG/Hb-MMT-PVA	CV	0.5	-	-	[24]
PG/Hb–DNA	DPV	2.9	-	DA, ascorbate, UA, catechol, cystine, epinephrine	[25]
GC/PADA-Au_{25} Ag_{75} NCs	Amperometry	0.01	3.77 nA nM^{-1}	glucose, urea, oxalate, NaCl, NO_3^-	[26]
GC/rGO–Au–TPDT	Amperometry	0.0065	0.598 nA nM^{-1}	glucose, urea, oxalate, NaCl	[27]
Pt/GO-PB	LSV	16.50	0.0091 μA μM^{-1}	Cl^-, NO_3^-, SO_3^{2-}, SO_4^{2-}, NO_2^-	[28]
Pt/GO-Fe_2O_3	LSV	13.04	0.016 μA μM^{-1}	Cl^-, NO_3^-, SO_3^{2-}, SO_4^{2-}, NO_2^-	[28]
GC/G-Nf	SWV	11.61	62 μA mM^{-1}	DA, AA	[29]
GC/rGO–Co_3O_4@Pt	Amperometry	1.73	0.026 μA μM^{-1}	DA, AA, UA, glucose, urea, NaCl	[12]
GC/Nf/G/AuNP	Amperometry	0.018	-	AA, xanthine, L-arginine, glycine, UA, NO_2^-	[30]
CF-(PAMAM/NiTsPc)	DPV	5.5	5.54 pA μM^{-1}	DA, NO_2^-, H_2O_2, norepinephrine, epinephrine, AA	[31]
GC/PtW/rGO-IL	Amperometry	0.00013	3.01 μA μM^{-1} cm^{-2}	DA, AA, UA	[32]
GC/Mb-AuNR/rGO	LSV	5.5	0.0539 μA μM^{-1}	$NaNO_3$, NaF, KCl, NH_4Cl, Na_2CO_3, glucose, AA, DA, UA, H_2O_2	[33]
GC/AuPt-rGO	Amperometry	0.00288	7.35 μA μM^{-1}	NO_3^-, K^+, SO_4^{2-}, Mg^{2+}, Cu^{2+}, Cys, AA, UA	[34]
GC/rGO-Nf@Au8	Amperometry	0.5	0.0621 μA μM^{-1}	DA, AA, UA, glucose, urea, NaCl	**This work**

Cyt c, cytochrome c; *SDS*, sodium dodecyl sulfate; *ITO*, indium tin oxide; *MPTS*, (3-mercaptopropyl)-trimethoxysilane; *FAuNPs*, fused spherical gold nanoparticles; *CPB*, cetylpyridinium bromide; *PAM*, polyacrylamide, *Fe(III)*, iron nanoparticles; *rGO*, reduced graphene oxide; *CeO_2*, ceria; *MMT*, montmorillonite; *PVA*, polyvinyl alcohol; *Hb*, hemoglobin; *PG*, pyrolytic graphite; *TPDT*, N1 -[3-(trimethoxysilyl)propyl];diethylene triamine; *Pt*, platinum; *GO*, graphene oxide; *PB*, prussion blue; *Fe_2O_3*, iron oxide; *Co_3O_4*, cobalt oxide; *CF*, carbon-fiber microelectrodes; *PAMAM*, polycationic dendrimer; *NiTsPc*, nickel phthalocyanine tetrasulfonated; *PtW*, platinumtungsten alloy nanoparticles; *IL*, ionic liquid, *SWV*, squarewave voltammetry; *DPV*, differential pulse voltammetry; *LSV*, linear scan voltammetry

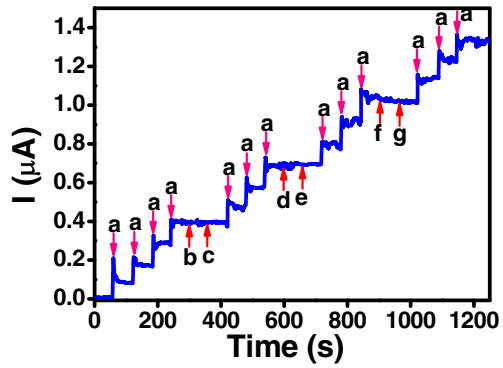

Fig. 6 Amperometry (I-t) response of **(a)** 1 μM NO_2^- at GC/rGO-Nf@Au8 modified electrode in 0.1 M phosphate buffer (pH 2.5) with successive additions of different interfering species such as **(b)** DA, **(c)** AA, **(d)** UA, **(e)** NaCl, **(f)** glucose, and **(g)** urea; each with 10 μM concentration. Applied potential was +0.8 V (vs. SCE)

owing to its immunity against the common interfering species.

Recovery test with real water samples

In order to certify the practicability of the GC/rGO-Nf@Au8 modified electrode in analytical applications, it was applied to detect NO in real water samples by the standard addition method. The water samples were used in real sample analysis in order to validate the sensor performance by calculating recovery % of known concentration of NO. The recoveries of different concentrations (10, 50, and 100 μM) of NO_2^- were detected in the tap and lake waters which were sampled from University of Malaya. The recovery values for three parallel measurements were calculated to evaluate the accuracy of the sensor and the results were listed in Table 2. It is clear that the sensor shows satisfactory results with the recovery in the range of 89–100.8% and RSD values in the range of from 0.6 to 2.1%, indicating that this method can be efficiently applied to determine in situ generated NO with good accuracy.

Table 2 Detection and recovery of NO in real water samples by using GC/rGO-Nf@Au8 modified electrode

Real samples	NO_2^- added (μM)	NO_2^- detected* (μM)	RSD (%)	Recovery (%)
Tap water	10	9.7	1.7	97
	50	50.4	0.7	100.8
	100	100.7	1.5	100.7
Lake water	10	8.9	2.1	89
	50	49.1	0.6	98.2
	100	97.9	0.6	97.9

* Average of three determinations

Conclusions

To sum up, the rGO-Nf@Au nanohybrids has been successfully synthesized by hydrothermal method and has been used to modify GCE before further applied to quantify NO in acidic solution (0.1 M phosphate buffer, pH 2.5). All the GC/rGO-Nf@Au (4, 8 and 12 mM) modified electrodes exhibit a good electrocatalytic activity towards the oxidation of NO. Among these electrodes, the GC/rGO-Nf@Au8 modified electrode displayed the best sensing performance for determination of NO. The GC/rGO-Nf@Au8 modified electrode has strong and sensitive current responses to NO with an amperometric detection limit of 5.0×10^{-7} M (S/*N* = 3) and a wide linear response ranging from 1 μM to 0.16 mM. It is noteworthy that this modified electrode is also highly resistant toward common interfering species such as DA, AA, UA, glucose, NaCl and urea, making it highly selective toward NO. Besides that, this modified electrode also demonstrating an acceptable reproducibility, repeatability, and excellent stability, which can be used as an amperometric sensor for determination of NO. The NO sensor presented in this work stands for its cost-effective synthesis of nanohybrid, easy fabrication of sensor electrode, interesting detection limit and selectivity compared to the other previously reported sensor electrodes. An excellent sensing performance shown by rGO-Nf@Au8 nanohybrids were attributed to the high conductivity and surface area provided by rGO-Nf sheets as well as the interface-dominated properties owned by AuNP. The strong synergistic effect between rGO-Nf and AuNP was further enhancing the sensing performance as it leads to the effective electron transfer, hence improved the sensitivity of the sensor electrode. The satisfactory results for NO analysis in tap and lake waters suggest that the sensor is suitable for practical applications. In view of the above results, it has proven that the rGO-Nf@Au8 nanohybrid has a great potential for the development of new electrochemical sensing devices especially for the in situ detection of NO.

Acknowledgements This project is supported by the Postgraduate Research Fund (PG122-2014b) from the University of Malaya.

Compliance with ethical standards The author(s) declare that they have no competing interests.

References

1. Ignarro LJ, Buga GM, Wood KS, Byrns RE, Chaudhuri G (1987) Endothelium-derived relaxing factor produced and released from artery and vein is nitric oxide. P Natl Acad Sci 84:9265–9269
2. Palmieri MC, Sell S, Huang X, Scherf M, Werner T, Durner J et al (2008) Nitric oxide-responsive genes and promoters in *Arabidopsis thaliana*: a bioinformatics approach. J Exp bot 59:177–186
3. Bredt DS, Snyder SH (1992) Nitric oxide, a novel neuronal messenger. Neuron 8:3–11

4. Smith AD, Taylor DR (2005) Is exhaled nitric oxide measurement a useful clinical test in asthma? Curr Opin Allergy Clin Immunol 5: 49–56
5. Avdagić N, Zaćiragić A, Babić N, Hukić M, Šeremet M, Lepara O et al (2013) Nitric oxide as a potential biomarker in inflammatory bowel disease. Bosnian J Basic Med Sci 13:5–9
6. Shiekh GA, Ayub T, Khan SN, Dar R, Andrabi KI (2011) Reduced nitrate level in individuals with hypertension and diabetes. J Cardiovasc Disease Res 2:172–176
7. Özden S, Tathpinar S, Bigçer N, Yaylali V, Yildirim C, Özbay D et al (2003) Basal serum nitric oxide levels in patients with type 2 diabetes mellitus and different stages of retinopathy. Can J Ophthalmol 38:393–396
8. Govindhan M, Liu Z, Chen A (2016) Design and electrochemical study of platinum-based nanomaterials for sensitive detection of nitric oxide in biomedical applications. Nano 6:211
9. Dang X, Hu H, Wang S, Hu S (2015) Nanomaterials-based electrochemical sensors for nitric oxide. Microchim Acta 182:455–467
10. Liu H, Weng L, Yang C (2017) A review on nanomaterial-based electrochemical sensors for H_2O_2, H_2S and NO inside cells or released by cells. Microchim Acta 184:1267–1283
11. Hu FX, Xie JL, Bao SJ, Yu L, Li CM (2015) Shape-controlled ceria-reduced graphene oxide nanocomposites toward high-sensitive in situ detection of nitric oxide. Biosens Bioelectron 70: 310–317
12. Shahid MM, Rameshkumar P, Pandikumar A, Lim HN, Ng YH, Huang NM (2015) An electrochemical sensing platform based on a reduced graphene oxide–cobalt oxide nanocube@ platinum nanocomposite for nitric oxide detection. J Mater Chem A 3:14458–14468
13. Yusoff N, Pandikumar A, Marlinda A, Huang N, Lim H (2015) Nanosized graphene/Nafion hybrid modified electrode for electrochemical detection of dopamine. Sci Adv Mater 7:2692–2703
14. Mhamane D, Ramadan W, Fawzy M, Rana A, Dubey M, Rode C et al (2011) From graphite oxide to highly water dispersible functionalized graphene by single step plant extract-induced deoxygenation. Green Chem 13:1990–1996
15. Xu Z, Huang Y, Min C, Chen L, Chen L (2010) Effect of γ-ray radiation on the polyacrylonitrile based carbon fibers. Radiat Phys Chem 79:839–843
16. Shen H-X, Yao J-L, Gu R-A (2009) Fabrication and characteristics of spindle Fe_2O_3@ Au core/shell particles. T Nonferr Metals Soc 19:652–656
17. Pocklanova R, Rathi AK, Gawande MB, Datta KKR, Ranc V, Cepe K et al (2016) Gold nanoparticle-decorated graphene oxide: synthesis and application in oxidation reactions under benign conditions. J Mol Catal A Chem 424:121–127
18. Kannan P, John SA (2010) Highly sensitive electrochemical determination of nitric oxide using fused spherical gold nanoparticles modified ITO electrode. Electrochim Acta 55:3497–3503
19. Chen X, Long H-Y, Wu W-L, Yang Z-S (2009) Direct electrochemical behavior of cytochrome c on sodium dodecyl sulfate modified electrode and its application to nitric oxide biosensor. Thin Sol Films 517:2787–2791
20. Santos VN, Cabral MF, Ferreira JS, Holanda AK, Machado SA, Sousa JR et al (2011) Study of a gold electrode modified by trans-$[Ru(NH_3)^4(Ist)SO_4]$+ to produce an electrochemical sensor for nitric oxide. Electrochim Acta 56:5686–5692
21. He X, Zhu L (2006) Direct electrochemistry of hemoglobin in cetylpyridinium bromide film: redox thermodynamics and electrocatalysis to nitric oxide. Electrochem Commun 8:615–620
22. Wang S, Lin X (2005) Electrodeposition of Pt–Fe (III) nanoparticle on glassy carbon electrode for electrochemical nitric oxide sensor. Electrochim Acta 50:2887–2891
23. Fan C, Liu X, Pang J, Li G, Scheer H (2004) Highly sensitive voltammetric biosensor for nitric oxide based on its high affinity with hemoglobin. Anal Chim Acta 523:225–228
24. Pang J, Fan C, Liu X, Chen T, Li G (2003) A nitric oxide biosensor based on the multi-assembly of hemoglobin/montmorillonite/polyvinyl alcohol at a pyrolytic graphite electrode. Biosens Bioelectron 19:441–445
25. Fan C, Li G, Zhu J, Zhu D (2000) A reagentless nitric oxide biosensor based on hemoglobin–DNA films. Anal Chim Acta 423:95–100
26. Viswanathan P, Manivannan S, Ramaraj R (2015) Polyelectrolyte stabilized bi-metallic Au/Ag nanoclusters modified electrode for nitric oxide detection. RSC Adv 5:54735–54741
27. Jayabal S, Viswanathan P, Ramaraj R (2014) Reduced graphene oxide–gold nanorod composite material stabilized in silicate sol–gel matrix for nitric oxide sensor. RSC Adv 4:33541–33548
28. Adekunle AS, Lebogang S, Gwala PL, Tsele TP, Olasunkanmi LO, Esther FO et al (2015) Electrochemical response of nitrite and nitric oxide on graphene oxide nanoparticles doped with Prussian blue (PB) and Fe_2O_3 nanoparticles. RSC Adv 5:27759–27774
29. Yusoff N, Pandikumar A, Marlinda AR, Huang NM, Lim HN (2015) Facile synthesis of nanosized graphene/Nafion hybrid materials and their application in electrochemical sensing of nitric oxide. Anal Method 7:3537–3544
30. Wang Y, Song B, Xu J, Hu S (2015) An amperometric sensor for nitric oxide based on a glassy carbon electrode modified with graphene, Nafion, and electrodeposited gold nanoparticles. Microchim Acta 182:711–718
31. Cancino J, Borgmann S, Machado SAS, Zucolotto V, Schuhmann W, Masa J (2015) Electrochemical sensor for nitric oxide using layered films composed of a polycationic dendrimer and nickel(II) phthalocyaninetetrasulfonate deposited on a carbon fiber electrode. Microchim Acta 182:1079–1087
32. Govindhan M, Chen A (2016) Enhanced electrochemical sensing of nitric oxide using a nanocomposite consisting of platinum-tungsten nanoparticles, reduced graphene oxide and an ionic liquid. Microchim Acta 183:2879–2887
33. Marlinda AR, Pandikumar A, Jayabal S, Yusoff N, Suriani AB, Huang NM (2016) Voltammetric determination of nitric oxide using a glassy carbon electrode modified with a nanohybrid consisting of myoglobin, gold nanorods, and reduced graphene oxide. Microchim Acta 183:3077–3085
34. Liu Z, Forsyth H, Khaper N, Chen A (2016) Sensitive electrochemical detection of nitric oxide based on AuPt and reduced graphene oxide nanocomposites. Analyst 141:4074–4083